Digital Object Identifier 10.1109/ECCE.2017.8096930

2017 IEEE Energy Conversion Congress and Exposition (ECCE)

Analysis and design of LCL filter based synchronverter

Roberto Rosso
Jair Cassoli
Soenke Engelken
Giampaolo Buticchi
Marco Liserre

Analysis and Design of LCL Filter Based Synchronverter

Roberto Rosso, Jair Cassoli, Soenke Engelken
WRD GmbH
Aurich, Germany
Email: roberto.rosso@enercon.de

Giampaolo Buticchi, Marco Liserre
Christian-Albrecht-University of Kiel
Chair of Power Electronics
Kiel, Germany
Email: gibu@tf.uni-kiel.de

***Abstract*—Electrical energy generation is evolving from centralized towards distributed energy resources (DER) like wind and solar power plants. In such power systems, new challenges arise for the design of voltage source converter (VSC) control strategies. In the last few years synchronverters have gained interest from the research community due to their capability of emulating synchronous machines (SMs) and therefore, in combination with energy storage systems, providing additional virtual inertia to the system. Furthermore, due to their intrinsic power synchronization mechanism, they are able to self-synchronize themselves to the grid without the need of a dedicated synchronization unit. In order to investigate the features of this type of controller, in this paper the small-signal analysis of a system consisting of a Synchronverter connected to the grid through an output LCL filter is presented. The results of the developed model will be compared first to time domain EMT simulations in MATLAB/Simulink/PLECS and subsequently to laboratory experiments, in order to prove their validity. The developed tool will be used for design purposes and to investigate the effects of parameters variation on the dynamic response of the system. Based on these considerations, a design procedure for a synchronverter will be presented.**

I. Introduction

The amount of power electronic converters connected to the grid is growing noticeably and this trend has concerned grid operators about the stability of the future power system. One of the main issues is related to the decrease of the total inertia of the system due to the replacement of standard generation units, mainly large SMs, with power electronics converters. During the last decade many researchers have focused their activity toward the development of inverter control strategies, which allow emulating the behaviour of standard SMs, the so called virtual synchronous machines (VSMs) [1]-[4]. Among the proposed control strategies, the synchronverter concept presented by Zhong et al. [3], [4] has been noted for its easy and intuitive structure and for being the first proposed control structure without the need of a dedicated synchronization unit both for synchronization to the main grid and during normal operation. Some VSM implementations use standard PI controllers in the inner voltage and current control loop and the tuning of the controller parameters has been performed by means of small-signal model analysis [2]. The issue of synchronverter design has recently been investigated in literature, also adopting the small-signal analysis approach [5]-[8]. However the presented small-signal models are only valid under certain assumptions. In this paper, a comprehensive small-signal model of a synchronverter connected to the grid through an output LCL filter is developed, which also considers the cross-coupling effects between active and reactive power and does not require any particular assumptions. The structure of the output inverter filter is left as general as possible, so that through parameter adjustments it is possible to model either L, LC or LCL filter. Filter parameters have been chosen so as to provide realistic results, but filter design is not the emphasis of this paper. The grid is modelled as a Thevenin equivalent, but a more detailed representation can be easily included.

The derived model is validated first through EMT time domain simulation in MATLAB/Simulink/PLECS and subsequently through experimental results. Based on the performed analysis, a design procedure for a Synchronverter taking into account filter and grid characteristics is presented and its effectiveness is proven by simulating three different filter and grid configurations and analyzing the response of the system when the proposed approach is adopted. The rest of the paper is structured as follow: in Section II an introduction to the VSM concept is presented, in Section III the derivation of the small-signal model of the system under study is reported and validated through EMT simulations. In Section IV the design procedure for a Synchronverter is presented, while in Section V experimental results are shown. In Section VI conclusions are drawn.

II. Overview on VSMs' characteristics

There are mainly two reasons why SMs are considered to be fundamental components of the power systems: the inertia of their rotating masses and their power synchronization mechanism.

The first work on VSM was presented by Hesse end Beck in 2007 [1], the so called VISMA concept, aiming at the development of a control to provide additional virtual inertia to the system. Other authors have focused on the same aspect and have developed control strategies based on the emulation of the swing equation of a synchronous machine [2]. In [9], D'Arco and Suul have demonstrated the equivalence between the small-signal response of the inertia emulation characteristic of VSM-based controls and conventional droop based controls for stand-alone and microgrid operation. In 2010 Zhang et al. presented the concept of "power synchronisation control"

for VSCs [10]. Observing that SMs are able to maintain their synchronism even in cases where standard current control structures using dedicated synchronisation units (such as PLLs) may encounter stability issues, a control concept based on the synchronisation mechanism typical of SM was proposed. The same principle was adopted by Rodriguez et al. in [11], where an active power synchronization loop was combined with a virtual output admittance. However, the synchronverter concept has been the first control structure presented in the literature, which completely overcomes the need for a PLL. Its design procedure was addressed at a later stage. The first attempt was presented in [5], where quasi-steady-state equations of the power transfer between two nodes connected by a resistive-inductive impedance have been used, but unfortunately such equations are not suitable for investigations of fast dynamic transients [10]. In [6], a parameter design approach based on a small-signal model analysis of a Synchronverter is presented. Several assumptions have to be made so that the model can be considered valid, e.g the system has to be connected to a grid with a short circuit ratio (SCR) higher then 10, which might not always be the case especially for applications where generation units are located at remote sites. In [8], an equivalent impedance model of a synchronverter is developed, which is suitable for impedance-based stability analysis. Also in this case some assumptions have to be made, namely the setpoint of the reactive power and its output value should be zero. The objective of this work is to develop a detailed small-signal model of a Synchronverter connected to the grid through an LCL filter in order to study the interactions between converter parameters and the system composed of the filter and the grid. For the analysis presented in this paper no assumption have to be made, neither on the power setpoint nor on the grid characteristics, providing a suitable procedure for synchronverter design.

III. Small-Signal model analysis

It has been demonstrated that small-signal model analysis is a practical and efficient tool for investigation of dynamic interactions between a converter's control and its output filter and in general between converters in a power system [12], [13]. In [2], the small-signal model approach has been adopted to analyse the eigenvalues of a VSM and their sensitivity with respect to system parameters. In [10], transfer functions of active power P versus load angle θ and reactive power P versus inverter voltage magnitude V are derived in dq coordinates. Only an inductive filter is supposed to be placed between the converter and the grid and cross-coupling effects between active and reactive power are usually neglected [6], [8]. In this paper an accurate small signal model of a synchronverter connected to the grid through an output LCL filter will be derived by splitting the system into two parts: the control and the plant composed of the filter and the grid. The equations of the two systems are linearized and their state space representations obtained. The simplified scheme of the system under study is presented in Fig. 1, while in Fig. 2 the inputs and outputs of the two linearized systems are shown.

A. Control

The inverter control structure analyzed in this paper has been presented in [3] and is shown in Fig. 1. The controller contains control loops for active power P and a reactive power Q. The active power loop emulates the frequency droop mechanism typical of a SM described by the well-known swing equation:

$$J\dot{\omega} = T_m - T_e - D_p\omega \ , \tag{1}$$

where J represents the mechanical (virtual) inertia, ω is the virtual rotor speed, D_p is the feedback gain that represents the (virtual) mechanical friction of the machine, T_e is the electrical torque and T_m is the mechanical torque. It is worth noticing that D_p does not only represent the virtual friction of the machine, but also the active power-frequency droop coefficient of the controller. T_m can be directly related to the electrical power setpoint P_{set} through the following equation:

$$T_m = \frac{P_{set}}{\omega_n} \ , \tag{2}$$

with ω_n being the nominal electrical frequency of the system (which usually coincides with ω_{ref}). Integrating ω, it is possible to obtain the virtual rotor angle θ, which will be used as reference for generating the virtual back-emf e^*. The reactive power-voltage droop control is conceptually similar to the active power-frequency droop. It reacts to a voltage deviation Δ_V from its nominal/reference value with a change of the reactive power setpoint Δ_Q according to the droop coefficient D_q:

$$\Delta_Q = -D_q\Delta_V \, . \tag{3}$$

Usually D_p and D_q are specified from requirements on the steady-state output response. The instantaneous reactive power measured at the output of the converter is then subtracted from the reactive power setpoint and added to the signal coming from the voltage droop. The resulting quantity is processed through an integrator with gain $1/K$ producing the control signal $M_f i_f$ also needed for the calculation of the virtual back-emf e^* of the machine. The calculated value directly forms the reference voltage for the generation of the inverter pulses, which avoids the need for a further internal current loop. However, this might be inconvenient for inverter current limitation purposes. Defining the following vectors:

$$\Delta x_c = \begin{bmatrix} \Delta M_f i_f \\ \Delta\omega \\ \Delta\theta \end{bmatrix}; \quad \Delta u_c = \begin{bmatrix} \Delta P_{set} \\ \Delta P \\ \Delta Q_{set} \\ \Delta Q \\ \Delta V_{PCC} \end{bmatrix}; \quad \Delta y_c = \begin{bmatrix} \Delta E_p \\ \Delta\theta \end{bmatrix}; \tag{4}$$

the system equations of the control can be written in the form of state space equations:

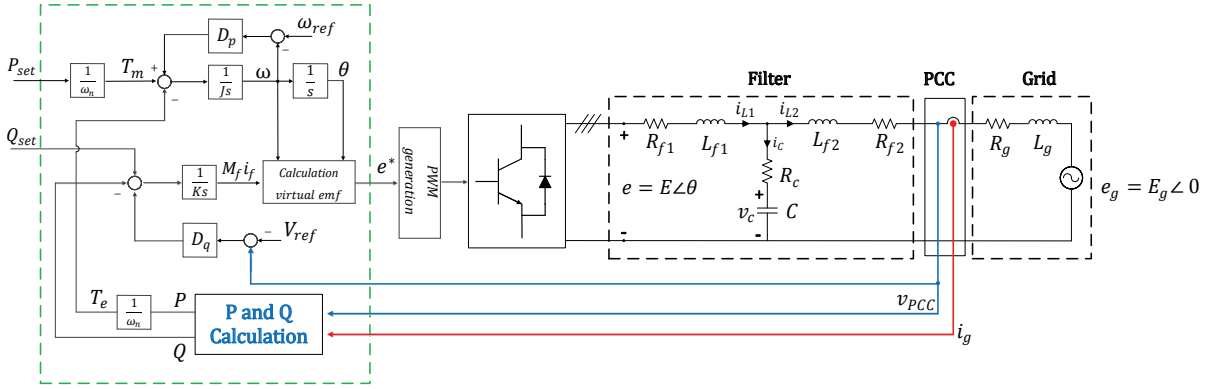

Figure 1: Simplified scheme of the system under study.

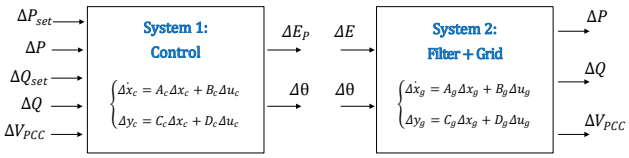

Figure 2: Inputs and outputs of the two linearized systems.

$$\begin{cases} \Delta\dot{x}_c = A_c\Delta x_c + B_c\Delta u_c \\ \Delta y_c = C_c\Delta x_c + D_c\Delta u_c \end{cases}, \tag{5}$$

where V_{PCC} is the voltage at the point of connection (PCC) and P and Q are the calculated active and reactive power, respectively, at the same point. Furthermore E_p represents the amplitude of the virtual back-emf, calculated by multiplying $M_f i_f$ by the virtual rotational frequency ω.

According to Fig.1 and adding small-signal perturbation terms to (1), results:

$$\frac{d\Delta\omega}{dt} = \frac{\Delta T_m}{J} - \frac{\Delta\omega}{J}D_p - \frac{\Delta P}{J\omega}. \tag{6}$$

Similarly the equation of the reactive power control loop can be obtained:

$$\frac{d\Delta M_f i_f}{dt} = \frac{\Delta Q_{set}}{K} - \frac{\Delta Q}{K} - \frac{\Delta V_{PCC}D_q}{K}. \tag{7}$$

Adding a small perturbation to θ yields:

$$\frac{d\Delta\theta}{dt} = \Delta\omega. \tag{8}$$

Finally E_p, obtained from the product between $M_f i_f$ and ω, can be linearized around the operating point identified by $M_f i_{f0}$ and ω_0 as:

$$\Delta E_p = M_f i_{f0}\ \Delta\omega + \Delta M_f i_f\ \omega_0. \tag{9}$$

According to (6)-(9), the state-space matrices A_c, B_c, C_c and D_c of (5) are obtained:

$$A_c = \begin{bmatrix} 0 & 0 & 0 \\ 0 & -\frac{D_p}{J} & 0 \\ 0 & 1 & 0 \end{bmatrix};\ B_c = \begin{bmatrix} 0 & 0 & \frac{1}{K} & -\frac{1}{K} & -\frac{D_q}{K} \\ \frac{1}{\omega_0 J} & -\frac{1}{\omega_0 J} & 0 & 0 & 0 \\ 0 & 0 & 0 & 0 & 0 \end{bmatrix};$$

$$C_c = \begin{bmatrix} \omega_0 & M_f i_{f0} & 0 \\ 0 & 0 & 1 \end{bmatrix};\quad D_c = \begin{bmatrix} 0^{2X5} \end{bmatrix}. \tag{10}$$

B. Filter and Grid

Similarly to the control equations, a state space representation of the plant composed of the inverter output filter and the grid will be obtained in this subsection. According to Fig. 1 and choosing i_{L1}, i_{L2} and v_c as state space variables, the following equations are valid:

$$\begin{cases} L_{f1}\frac{di_{L1}}{dt} = e - v_c - R_c(i_{L1} - i_{L2}) - R_{f1}i_{L1} \\ C\frac{dv_c}{dt} = i_{L1} - i_{L2} \\ (L_{f2} + L_g)\frac{di_{L2}}{dt} = v_c - e_g + R_c(i_{L1} - i_{L2}) - (R_{f2} + R_g)i_{L2} \end{cases}. \tag{11}$$

Writing (11) in dq coordinates [14] and adding small signal perturbations yields:

$$\begin{cases} L_{f1}\frac{d\Delta i_{L1d}}{dt} = -E_0\sin\theta_0\Delta\theta - \Delta E\cos\theta_0 - \Delta v_{cd} + \\ \qquad -R_{f1}\Delta i_{L1d} - R_c(\Delta i_{L1d} - \Delta i_{L2d}) + \omega_0 L_{f1} i_{L1q} \\ L_{f1}\frac{d\Delta i_{L1q}}{dt} = E_0\cos\theta_0\Delta\theta + \Delta E\sin\theta_0 - \Delta v_{cq} + \\ \qquad -R_{f1}\Delta i_{L1q} - R_c(\Delta i_{L1q} - \Delta i_{L2q}) - \omega_0 L_{f1} i_{L1d} \end{cases}; \tag{12}$$

$$\begin{cases} C\frac{d\Delta v_{cd}}{dt} = \Delta i_{L1d} - \Delta i_{L2d} + \omega_0 C\Delta v_{cq} \\ C\frac{d\Delta v_{cq}}{dt} = \Delta i_{L1q} - \Delta i_{L2q} - \omega_0 C\Delta v_{cd} \end{cases}; \tag{13}$$

$$\begin{cases} (L_{f2} + L_g)\frac{d\Delta i_{L2d}}{dt} = \Delta v_{cd} + R_c(\Delta i_{L1d} - \Delta i_{L2d}) + \\ \qquad -(R_{f2} + R_g)\Delta i_{L2d} + \omega_0(L_{f2} + L_g)\Delta i_{L2q} \\ (L_{f2} + L_g)\frac{d\Delta i_{L2q}}{dt} = \Delta v_{cq} + R_c(\Delta i_{L1q} - \Delta i_{L2q}) + \\ \qquad -(R_{f2} + R_g)\Delta i_{L2q} - \omega_0(L_{f2} + L_g)\Delta i_{L2d} \end{cases}; \tag{14}$$

where all the quantities with the subscript "0" indicate the values at the operating point and the procedure to calculate their values will be presented in the following. According to Fig. 1, active and reactive power injected into the grid can be expressed as:

$$\begin{cases} P = \frac{3}{2}(i_{L2d}v_{PCCd} + i_{L2q}v_{PCCq}) \\ Q = \frac{3}{2}(i_{L2d}v_{PCCq} - i_{L2q}v_{PCCd}) \end{cases}, \quad (15)$$

where v_{PCCd} and v_{PCCq} are the d and q components of the voltages at the PCC respectively, while i_{L2d} and i_{L2q} are the components of the current flowing into the grid, which in this case corresponds to the current flowing through L_{f2} and L_g. Linearizing eq.(15) yields:

$$\begin{cases} \Delta P = \frac{3}{2}(I_{L2d0}\Delta v_{PCCd} + V_{PCCd0}\Delta i_{L2d} + \\ \qquad + V_{PCCq0}\Delta i_{L2q} + I_{L2q0}\Delta v_{PCCq}) \\ \Delta Q = \frac{3}{2}(V_{PCCq0}\Delta i_{L2d} + I_{L2d0}\Delta v_{PCCq} + \\ \qquad - V_{PCCd0}\Delta i_{L2q} + I_{L2q0}\Delta v_{PCCd}) \end{cases}, \quad (16)$$

where

$$\begin{cases} \Delta v_{PCCd} = \Delta v_{cd} + R_c(\Delta i_{L1d} - \Delta i_{L2d}) + \\ \qquad - R_{f2}\Delta i_{L2d} - L_{f2}\frac{di_{L2d}}{dt} + \omega_0 L_{f2}\Delta i_{L2q} \\ \Delta v_{PCCq} = \Delta v_{cq} + R_c(\Delta i_{L1q} - \Delta i_{L2q}) + \\ \qquad - R_{f2}\Delta i_{L2q} - L_{f2}\frac{di_{L2q}}{dt} - \omega_0 L_{f2}\Delta i_{L2d} \end{cases}. \quad (17)$$

The voltage at the PCC can be expressed in dq coordinates as:

$$V_{PCC} = \sqrt{V_{PCCd}^2 + V_{PCCq}^2}, \quad (18)$$

and the linearization of (18) produces:

$$\Delta V_{PCC} = \frac{V_{PCCd0}\Delta v_{PCCd} + V_{PCCq0}\Delta v_{PCCq}}{\sqrt{V_{PCCd0}^2 + V_{PCCq0}^2}}. \quad (19)$$

Now the state space representation of System 2 in Fig. 2 can be obtained:

$$\begin{cases} \dot{\Delta x_g} = A_g\Delta x_g + B_g\Delta u_g \\ \Delta y_g = C_g\Delta x_g + D_g\Delta u_g \end{cases}, \quad (20)$$

where Δx_g represents the state vector, Δu_g the input vector and Δy_g the output vector, defined as follows:

$$\Delta x_g = \begin{bmatrix} \Delta i_{L1d} \\ \Delta i_{L1q} \\ \Delta v_{cd} \\ \Delta v_{cq} \\ \Delta i_{L2d} \\ \Delta i_{L2q} \end{bmatrix}; \quad \Delta u_g = \begin{bmatrix} \Delta E \\ \Delta\theta \end{bmatrix}; \quad \Delta y_g = \begin{bmatrix} \Delta P \\ \Delta Q \\ \Delta V_{PCC} \end{bmatrix}; \quad (21)$$

The state space matrices A_g, B_g, C_g and D_g are defined as:

$$A_g = \begin{bmatrix} 0 & \omega_0 & \frac{1}{C} & 0 & -\frac{1}{C} & 0 \\ -\omega_0 & 0 & 0 & \frac{1}{C} & 0 & -\frac{1}{C} \\ -\frac{1}{L_{f1}} & 0 & -\frac{R_{f1}+R_c}{L_{f1}} & \omega_0 & \frac{R_c}{L_{f1}} & 0 \\ 0 & -\frac{1}{L_{f1}} & -\omega_0 & -\frac{R_{f1}+R_c}{L_{f1}} & 0 & \frac{R_c}{L_{f1}} \\ \frac{1}{L_g+L_{f2}} & 0 & \frac{R_c}{L_g+L_{f2}} & 0 & -\frac{R_c+R_{f2}+R_g}{L_g+L_{f2}} & \omega_0 \\ 0 & \frac{1}{L_g+L_{f2}} & 0 & \frac{R_c}{L_g+L_{f2}} & -\omega_0 & -\frac{R_c+R_{f2}+R_g}{L_g+L_{f2}} \end{bmatrix};$$

$$B_g^T = \begin{bmatrix} 0 & 0 & \frac{\cos\theta_0}{L_{f1}} & \frac{\sin\theta_0}{L_{f1}} & 0 & 0 \\ 0 & 0 & -\frac{V_0\sin\theta_0}{L_{f1}} & \frac{V_0\cos\theta_0}{L_{f1}} & 0 & 0 \end{bmatrix};$$

$$C_g = \begin{bmatrix} \alpha_1 & \alpha_2 & \alpha_3 & \alpha_4 & \alpha_5 & \alpha_6 \\ \beta_1 & \beta_2 & \beta_3 & \beta_4 & \beta_5 & \beta_6 \\ \gamma_1 & \gamma_2 & \gamma_3 & \gamma_4 & \gamma_5 & \gamma_6 \end{bmatrix}; \quad D_g = \begin{bmatrix} 0^{3X2} \end{bmatrix}; \quad (22)$$

where the elements of C_g are reported in the Appendix. The initial operating conditions can be obtained by solving the following system of equations obtained from the linearization process of (12)-(14) and (17):

$$\begin{cases} E_g = V_{PCCd0} - R_g I_{L2d0} + \omega_0 L_g I_{L2q0} \\ 0 = V_{PCCq0} - R_g I_{L2q0} - \omega_0 L_g I_{L2d0} \\ E_0\cos\theta_0 = V_{cd0} + (R_c + R_{f1})I_{L1d0} - R_c I_{L2d0} - \omega_0 L_{f1} I_{L1q0} \\ E_0\sin\theta_0 = V_{cq0} + (R_c + R_{f1})I_{L1q0} - R_c I_{L2q0} + \omega_0 L_{f1} I_{L1d0} \\ 0 = I_{L1d0} - I_{L2d0} + \omega_0 C V_{cq0} \\ 0 = I_{L1q0} - I_{L2q0} - \omega_0 C V_{cd0} \\ E_g = V_{cd0} + R_c I_{L1d0} - R_s I_{L2d0} + \omega_0(L_g + L_{f2})I_{L2q0} \\ 0 = V_{cq0} + R_c I_{L1q0} - R_s I_{L2q0} - \omega_0(L_g + L_{f2})I_{L2d0} \end{cases}, \quad (23)$$

where R_s represents the sum of R_c, R_{f2} and R_g.

C. Validation against EMT-Simulations

In order to validate the derived small-signal model, the system shown in Fig. 1 was simulated in MATLAB/Simulink/PLECS and the results are compared to the ones obtained from the frequency-domain analysis. Two different time-domain models have been implemented: first the inverter was modeled just as a voltage source, neglecting therefore the high order frequency effects due to the PWM modulation and the switching of the converter and subsequently a more detailed converter model was included in the simulation. The dynamic behaviour of the transfer function $\frac{\Delta P}{\Delta P_{set}}$ and the cross-coupling effect to the reactive power $\frac{\Delta Q}{\Delta P_{set}}$ due to a step of the active power setpoint ΔP_{set} of 0.3 pu were observed. Afterwards a step of ΔQ_{set} of the same magnitude was simulated and the dynamic behaviour of the transfer functions $\frac{\Delta Q}{\Delta Q_{set}}$ and $\frac{\Delta P}{\Delta Q_{set}}$ in the three different models were compared, with the results shown in Fig. 3. It can be clearly seen that the developed small signal-model is able to predict correctly the dynamic behaviour of the system. The yellow dashed curve in Fig. 3 is in almost all the cases overlapping the red curve representing the results of the EMT average

model where the converter is simulated using a voltage source. Also the cross-coupling effects are modeled correctly. It is worth pointing out that in Fig. 3 (d) the steady-state value of the reactive power is not 0.3 pu as the given setpoint due to the voltage droop controller, which adjusts the reactive power setpoint according to the voltage deviation at the PCC.

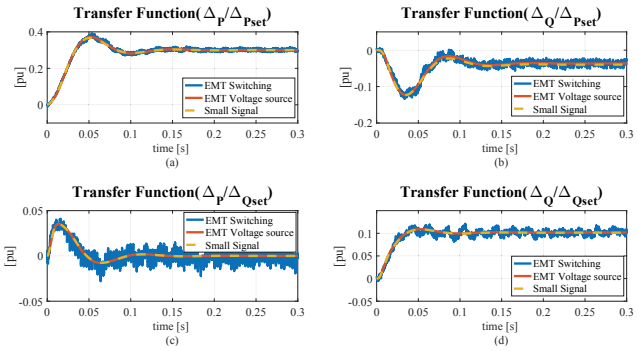

Figure 3: Comparison EMT Simulations vs. Small signal model: (blue) EMT switching model, (red) EMT average model, (yellow) analytical model. (a) $\frac{\Delta_P}{\Delta P_{set}}$, (b) $\frac{\Delta_Q}{\Delta P_{set}}$, (c) $\frac{\Delta_P}{\Delta Q_{set}}$, (d) $\frac{\Delta_Q}{\Delta Q_{set}}$.

Simulation parameters are provided in Table I.

Table I: Simulation parameters

Description	Symbol	Value
Inverter rated power	S_n	300 KVA
Grid short-circuit Ratio	SCR	10
Grid X/R Ratio	X/R	5
Line-to-line voltage	V_{LL}	400 V (rms)
Rated grid frequency	f_g	50 Hz
Inverter switching frequency	f_{sw}	4 KHz
Grid inductance	L_g	0.1 pu
Inverter-side filter inductance	L_{f1}	0.08 pu
Grid-side filter inductance	L_{f2}	0.02 pu
Grid resistance	R_g	0.02 pu
Inverter-side filter resistance	R_{f1}	0.05 pu
Grid-side filter resistance	R_{f2}	0.05 pu
Capacitor damping resistance	R_c	0.18 pu
Filter capacitor	C	0.05 pu
Virtual inertia	J	0.6687
P-Droop coefficient	D_p	60.8
Q-Droop coefficient	D_q	18371
Q loop integrator gain	K	57715

IV. Controller Design

In this section a synchronverter design procedure will be proposed assuming that the main objective is to use the Synchronverter control structure in order to take advantage of the intrinsic power synchronization mechanism of the VSM and not necessarily the inertia emulation, which could also be achieved with other approaches and relies on available storage. The performance of the control will be evaluated in terms of rise time, overshoot and settling time. The controller parameters which need to be tuned are the active and reactive power droop coefficients D_p and D_q, respectively, the virtual inertia J and the integrator gain K.

The concept of droop controllers is a well-known characteristic of governors for Synchronous generators. Typical values for the steady state droop are around 5% [15]. It can be assumed that these two parameters are already fixed due to specifications on the steady-state values and therefore only the virtual inertia J for the frequency loop and K for the voltage loop can be adjusted to improve the dynamic behaviour. By the way the presented design procedure can be adopted even in the case that the four parameters are freely adjustable.

A. Active power loop

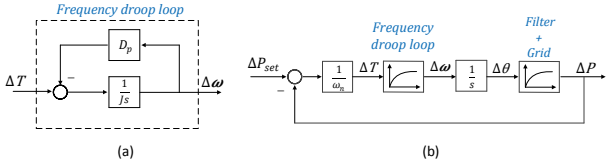

Figure 4: (a) simplified frequency droop loop, (b) simplified active power loop.

In Fig. 4(a) a simplified scheme of the Synchronverter's frequency droop loop is shown, which can be described as a first order transfer function having gain K_f and time constant τ_f:

$$K_f = \frac{1}{D_p} \quad ; \quad \tau_f = \frac{J}{D_p}. \tag{24}$$

In Fig. 4(b) a simplified scheme of the active power closed loop is reported. Bearing in mind that the virtual torque can be obtained by dividing the power by the nominal frequency ω_n, the plant composed of the filter and the grid (indicated as System 2 in Fig. 2) will be described dynamically by the transfer function $\frac{\Delta_P}{\Delta_\theta}$ obtained in the previous section. Each of the transfer functions of System 2 can be approximated by an equivalent first order transfer function by performing model order reduction. The system has six poles; two of them have the same time constant τ_{ref1}, while the other four have time constant τ_{ref2}. The transfer function $\frac{\Delta_P}{\Delta_\theta}$ of System 2 can be then approximated by a simple first order transfer function:

$$PT1_P(s) = \frac{G_p}{1 + s\ \tau_{refp}}\ , \tag{25}$$

where G_P is the steady-state value of $\frac{\Delta_P}{\Delta_\theta}$ and τ_{refp} the time constant of the dominant pole of the transfer function, which can be easily identified by observing its step response.

In order to improve the dynamic response of the frequency droop loop, τ_f shall be chosen sufficiently smaller then τ_{refp}, (eg. $\tau_f = \tau_{refp}/10$). With this choice the active power loop can be approximated by the second order transfer function reported below:

$$P_{app}(s) = \frac{1}{T_p^2 s^2 + 2\zeta_p T_p s + 1}\ , \tag{26}$$

where T_p and ζ_p represent the inverse natural frequency and the damping ratio respectively, defined as:

$$T_p = \sqrt{\frac{\tau_{refp}\omega_n D_p}{G_p}} \quad ; \quad \zeta_p = \frac{1}{2}\sqrt{\frac{D_p\omega_n}{\tau_{refp}}}. \tag{27}$$

Looking at (27) it can be clearly seen that D_P is the only control parameter influencing ζ_p. In the case that this value is already defined in order to comply with steady-state performance requirements, the damping of the active power loop cannot be changed. This issue is already known and [7] proposed a modification of the synchronverter's structure in order to improve the dynamic response of the active power loop. However, this has not been considered in the present work. In case that D_P and J are freely adjustable, it is recommended to choose them so as to have $\tau_f << \tau_{ref}$ and $\zeta_P = \frac{1}{\sqrt{2}}$ [16].

B. Reactive power loop

Concerning the $Q-V$ droop, two different loops can be identified, namely a reactive power and a voltage control loop, shown in Fig. 5(a) and (b) respectively. The loop in 5(a) can be considered as the case when the voltage droop control is deactivated. Similarly as for the active power loop, the two loops are reduced to simple second order transfer functions.

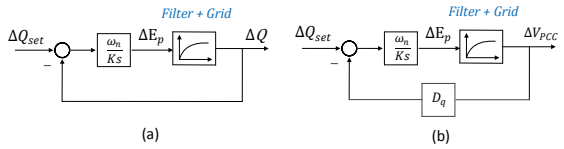

Figure 5: (a) simplified reactive power loop scheme, (b) simplified V_{PCC} loop scheme.

Also in this case the behaviour of $\frac{\Delta_Q}{\Delta E_p}$ and $\frac{\Delta V_{PCC}}{\Delta E_p}$ of System 2, can be approximated by reduced first order transfer functions indicated as $PT1_Q$ and $PT1_V$:

$$PT1_Q(s) = \frac{G_q}{1+s\ \tau_{refq}} \quad ; \quad PT1_V(s) = \frac{G_v}{1+s\ \tau_{refv}}, \tag{28}$$

where G_q and G_v are the steady-state values of $\frac{\Delta_Q}{\Delta E_p}$ and $\frac{\Delta V_{PCC}}{\Delta E_p}$ respectively and the τ_{refQ} and τ_{refV} are the dominant pole time constants identified in the same way as done for (27). The two closed loops are second-order transfer functions with the following damping factors:

$$\zeta_q(s) = \frac{1}{2}\sqrt{\frac{K}{\tau_{refq}\omega_n G_q}} \quad ; \quad \zeta_v(s) = \frac{1}{2}\sqrt{\frac{K}{\tau_{refv}\omega_n D_q G_q}}. \tag{29}$$

If D_q can be arbitrarily modified, K and D_q can be chosen such that $\zeta_q = \zeta_v = \frac{1}{\sqrt{2}}$. Otherwise two different values of K will be found, which might differ noticeably from each other. It is recommended to choose the highest of the two as reference value for K, as it will become more clear looking at the simulation results presented in the following.

C. Simulation Results

In order to show the effectiveness of the proposed design procedure, three different cases with different filter and grid parameters have been analyzed. First the case of a strong grid with a properly tuned LCL filter was taken into account, then the case of a weak grid with low short circuit ratio (SCR) and low $\frac{X}{R}$ ratio and finally the case of a weak grid with an over dimensioned filter. The optimal parameters J_{opt} and K_{opt} have been calculated according to the proposed approach, while D_p and D_q have been assumed both equal to 5 %. First the dynamic response of the system for a step of active power of 0.3 pu was observed varying the value of J within the range $[\frac{J_{opt}}{10}\ ;\ 10\ J_{opt}]$, whereas K was set to the calculated optimal value. Subsequently the response of the system to a step of reactive power of the same amplitude was simulated and the dynamic response of the system varying K in the range $[\frac{K_{opt}}{10}\ ;\ 10\ K_{opt}]$ was observed, maintaining instead J fixed at the calculated optimal value.

In Fig. 6 simulation results using the full model are reported showing the dynamic response of the system for the three examined cases. The direction of the arrows indicates the increment of the indicated parameters, the red curve is the response obtained by setting the parameters obtained from the proposed design procedure, while green curves are for values below the optimal one and blue curves for values above it. In Table II simulation parameters for the three examined cases are reported.

Table II: Parameters of the three simulated cases

Parameter	Case 1	Case 2	Case 3
S_n (KVA)	300	300	3
SCR	20	3	5
X/R	10	1	2
V_{LL} (V rms)	400	400	400
f_g (Hz)	50	50	50
L_g (pu)	0.05	0.235	0.1789
L_{f1} (pu)	0.08	0.08	0.3979
L_{f2} (pu)	0.02	0.02	0.1
R_g (pu)	0.005	0.235	0.09
R_{f1} (pu)	0.01	0.01	0.05
R_{f2} (pu)	0.01	0.01	0.05
R_c (pu)	0.18	0.18	0.93
C (pu)	0.05	0.05	0.25
J_{opt}	0.0742	0.2535	0.119
D_p	60.8	60.8	0.608
D_q	18371	18371	183.7
K_{opt}	71563	16956	178.27

V. Experimental Results

In order to validate the analytical investigation carried out in this work, laboratory experiments have been performed and the results will be presented in the following. In Fig. 7(a) a simplified scheme of the experimental setup is depicted, while in Fig. 7(b) the laboratory environment is shown. Two inverters sharing the same DC-Link have been used for the purposes of the tests. One inverter connected to an LCL filter and a transformer were used to emulate the VSM, while the second inverter was used to emulate the grid and was controlled in open loop in order to avoid unwanted interferences between the two controllers. The grid emulator was connected to the PCC through an L filter and therefore the emulated grid is mainly inductive. Furthermore each converter is equipped with

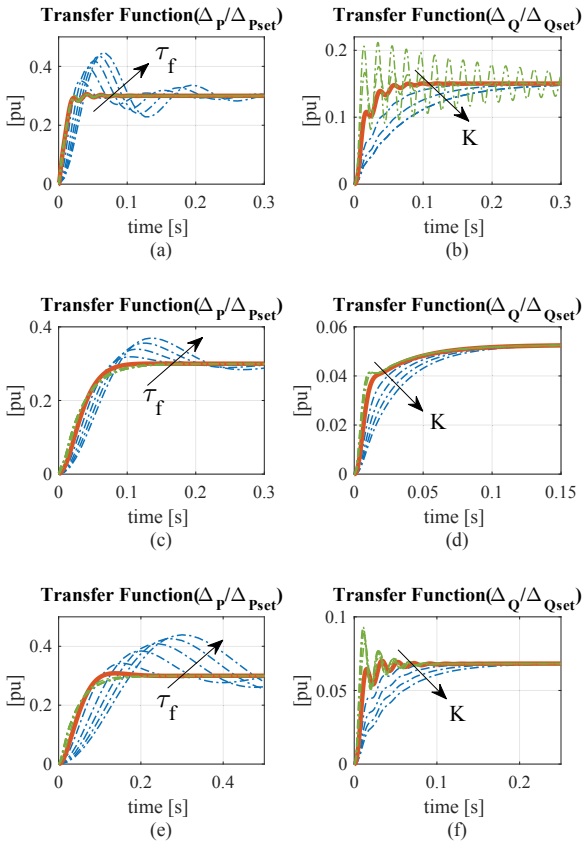

Figure 6: Effects of τ_f on the dynamic response of $\frac{\Delta_P}{\Delta P_{set}}$ for the three examined cases: (a) case 1, (c) case 2, (e) case 3. Effects of K on the dynamic response of $\frac{\Delta_Q}{\Delta Q_{set}}$ for the three examined cases: (b) case 1, (d) case 2, (f) case 3. (red): response with the optimal value obtained by using the proposed procedure,(green): response with values below the optimal one, (blue): response with values above the optimal one.

an additional transformer in order to provide galvanic isolation. The controls of the converters have been implemented in a dSPACE Control Desk ds1006. The parameters of the system and of the control used for the tests are reported in Table III. A comparison between measurements, simulations with the EMT average model and the response of the small-signal model is shown in Fig. 8. The dynamic behaviour of the transfer functions $\frac{\Delta_P}{\Delta P_{set}}$ and $\frac{\Delta_Q}{\Delta P_{set}}$ for a step of the power setpoint of 0.3 pu (900 W) and three different values of the parameter K can be seen. It is clearly visible how the system becomes less damped by decreasing K, reaching the instability for a value of K=25. A good match between measurements and simulations can be observed in Fig. 8, except for some discrepancies especially for K= 500. The response of the small signal model matches almost perfectly with the EMT average model. Therefore the mismatch is probably due to parameter uncertainties and the presence of the two transformers, which have been modeled by means of their leakage inductances assumed as part of the equivalent grid. The model correctly predicts the instability confirming that the developed tool is suitable for the purposes of the investigation presented in this paper.

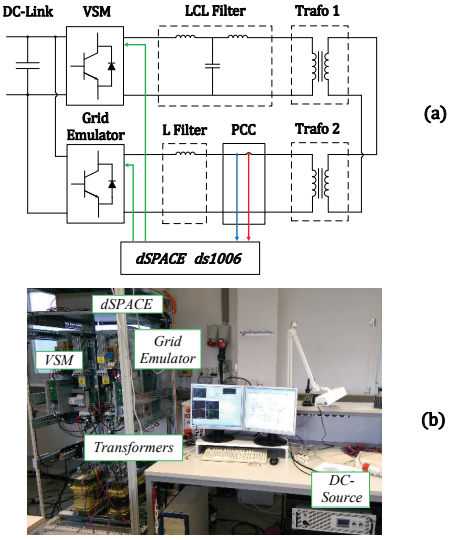

Figure 7: (a) Scheme of the laboratory setup, (b) picture of the experimental setup.

Table III: Parameters experimental setup

Description	Symbol	Value
Inverter rated power	S_n	3 KVA
Line-to-line voltage	V_{LL}	400 V (rms)
Rated grid frequency	f_g	50 Hz
Inverter switching frequency	f_{sw}	5 KHz
Grid inductance	L_g	0.035 pu
Inverter-side filter inductance	L_{f1}	0.03 pu
Grid-side filter inductance	L_{f2}	0.003 pu
Transformer inductance	$L_{T1} = L_{T2}$	0.003 pu
Grid resistance	R_g	0.022 pu
Inverter-side filter resistance	R_{f1}	0.0375 pu
Grid-side filter resistance	R_{f2}	0.018 pu
Capacitor damping resistance	R_c	0.037 pu
Filter capacitor	C	0.025 pu
Virtual inertia	J	4.9e-3
P-Droop coefficient	D_p	0.679
Q-Droop coefficient	D_q	183.71

VI. Conclusion

In this paper the small-signal model implementation of a Synchronverter connected to the grid through an output LCL filter is presented. The procedure for deriving the equations of the model was introduced and explained in detail. The filter configuration was left as general as possible so that through proper parameter choice is it possible to simulate either an L, LC or LCL output inverter filter. EMT time-domain simulations and laboratory experiments were performed in order to validate the derived small-signal model. Controller design was addressed in this work. The single controller loops were reduced to equivalent second order transfer functions in order to achieve optimal parameter tuning. The results obtained for three different configurations show the validity of the proposed approach, which provides a straightforward procedure for synchronverter design.

Appendix

The elements of C_g are reported below:

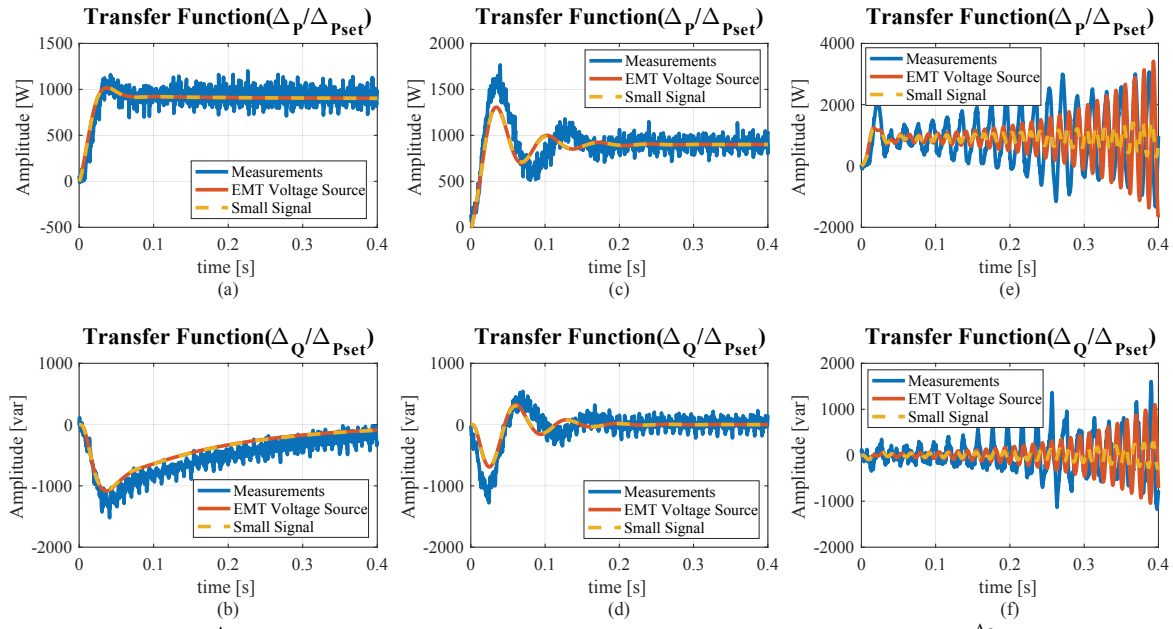

Figure 8: Dynamic behaviour of $\frac{\Delta_P}{\Delta P_{set}}$ for a step of 0.3 pu; (a) K = 7000, (c) K = 500, (e) K = 25. Dynamic behaviour of $\frac{\Delta_Q}{\Delta P_{set}}$ for a step of 0.3 pu; (b) K = 7000, (d) K = 500, (f) K = 25.

$$
\begin{cases}
\alpha_1 = \frac{3}{2}\frac{I_{L2d0}L_g}{L_g+L_{f2}} = \beta_2 \\
\alpha_2 = \frac{3}{2}\frac{I_{L2q0}L_g}{L_g+L_{f2}} = -\beta_1 \\
\alpha_3 = \frac{3}{2}\frac{I_{L2d0}R_cL_g}{L_g+L_{f2}} = \beta_4 \\
\alpha_4 = \frac{3}{2}\frac{I_{L2q0}R_cL_g}{L_g+L_{f2}} = -\beta_3 \\
\alpha_5 = \frac{3}{2}\left[I_{L2d0}\left(\frac{L_{f2}R_g-L_gR_{f2}-R_cL_g}{L_g+L_{f2}}\right)+V_{PCCd0}\right] \\
\alpha_6 = \frac{3}{2}\left[I_{L2q0}\left(\frac{L_{f2}R_g-L_gR_{f2}-R_cL_g}{L_g+L_{f2}}\right)+V_{PCCq0}\right] \\
\beta_5 = -\frac{3}{2}\left[I_{L2q0}\left(\frac{L_{f2}R_g-L_gR_{f2}-R_cL_g}{L_g+L_{f2}}\right)-V_{PCCq0}\right] \\
\beta_6 = \frac{3}{2}\left[I_{L2d0}\left(\frac{L_{f2}R_g-L_gR_{f2}-R_cL_g}{L_g+L_{f2}}\right)-V_{PCCd0}\right] \\
\gamma_1 = \frac{V_{PCCd0}}{\sqrt{V_{PCCd0}^2+V_{PCCq0}^2}}\frac{L_g}{L_g+L_{f2}} \\
\gamma_2 = \frac{V_{PCCq0}}{\sqrt{V_{PCCd0}^2+V_{PCCq0}^2}}\frac{L_g}{L_g+L_{f2}} \\
\gamma_3 = \frac{V_{PCCd0}}{\sqrt{V_{PCCd0}^2+V_{PCCq0}^2}}\frac{R_cL_g}{L_g+L_{f2}} \\
\gamma_4 = \frac{V_{PCCq0}}{\sqrt{V_{PCCd0}^2+V_{PCCq0}^2}}\frac{R_cL_g}{L_g+L_{f2}} \\
\gamma_5 = \frac{V_{PCCd0}}{\sqrt{V_{PCCd0}^2+V_{PCCq0}^2}}\frac{R_gL_{f2}-R_{f2}L_g-R_cLg}{L_g+L_{f2}} \\
\gamma_6 = \frac{V_{PCCq0}}{\sqrt{V_{PCCd0}^2+V_{PCCq0}^2}}\frac{R_gL_{f2}-R_{f2}L_g-R_cLg}{L_g+L_{f2}}
\end{cases}
$$

REFERENCES

[1] H.-P. Beck, R. Hesse, *"Virtual synchronous machine"*, in Proceedings of the 9th International Conference on Electrical Power Quality and Utilization, Oct. 2007.

[2] S. D'Arco, J. A. Suul, O. B. Fosso, *"Small-signal Modelling and Parametric Sensitivity of a Virtual Synchronous Machine"*, Power System Computation Conference (PSCC), pp. 1-9, 2014.

[3] Q.- C. Zhong, G. Weiss, *"Synchronverters: inverters that mimic synchronous generators"*, IEEE Trans. On Ind. Electron. , Vol. 58, no. 4, pp. 1259-1267, Apr. 2011.

[4] Q.- C. Zhong, P.-L. Nguyen, Z. Ma, W. Sheng, *"Self-synchronized Synchronverters: inverters without a dedicated synchronization unit"*, IEEE Trans. On Power Electron. , Vol. 29, no. 2, pp. 617-630, Feb. 2014.

[5] Z. Wei, C. Jie, G. Chunying, *"Small signal modeling and analysis of Synchronverters"*, Future Energy Electronics Conference (IFEEC), 2015 IEEE 2nd International, pp.1-5, 1-4 Nov. 2015.

[6] H. Wu, X. Ruan, D. Yang, X. Chen, W. Zhao, Z. Lv, Q.-C. Zhong, *"Small-Signal modeling and parameters design for virtual synchronous generators"*, IEEE Trans. On Ind. Electr., Vol. 63, no. 7, pp.4292-4303, July 2016.

[7] S. Dong, Y. C. Chen, *"Adjusting Synchronverter dynamic response speed via damping correction loop"*, IEEE Transactions on Energy Conversion, Vol. 32, no. 2, pp.608-619, July 2017.

[8] M. Amin and M. Molinas, *"Self-synchronization of wind farms in MMC-based HVDC system"*, 2016 IEEE Electrical Power and Energy Conference (EPEC), Ottawa, ON, 2016, pp. 1-6.

[9] S. D'Arco, J. A. Suul, *"Virtual synchronous machines Classification of implementation and analysis of equivalence to droop controllers for microgrids"*, PowerTech, 2013 IEEE Grenoble , pp. 1-7, 16-20 Jun. 2013.

[10] L. Zhang, L. Harnefors, H. P. Nee *"Power Synchronization Control of Grid-Connected Voltage Source Converters"*, IEEE Trans. On Power Systems, Vol. 25, no. 2, pp. 809-820, May 2010.

[11] P. Rodriguez, I. Candela, C. Citro, J. Rocabert, A. Luna, *"Control of grid-connected converters based on a virtual admittance control loop"*, 15th European Conf. on Power Electronics and Applications (EPE), pp.1-10, Sep. 2013.

[12] J. Sun, *"Small-Signal Methods for AC Distributed Power Systems-A Review"*, IEEE Trans. On Power Electr., Vol. 24, no. 11, pp.2545-2553, November 2009.

[13] X. Wang, F. Blaabjerg and W. Wu, *"Modeling and analysis of harmonic stability in an AC power-electronics-based power system"*, IEEE Trans. On Ind. Electr., Vol. 29, no. 12, pp.6421-6432, December 2014.

[14] P. C. Krause, O. Wasyrczuk, S. D. Sudhoff, *"Analysis of Electrical Machinery and Drive Systems"*, Wiley-IEEE Press, 2013.

[15] P. Kundur, *"Power System Stability and Control"*, McGraw-Hill, Inc. 1994.

[16] D. Schroeder, *"Elektrische Antriebe 2, Regelung von Antriebssystemen"*, 2nd ed., Germany: Springer-Verlag, 2001.